Citation: Sensors & Actuators: B. Chemical 367 (2022) 132062

Near-field Electrospinning of Polymer/Phage Whispering Gallery Mode Microfiber Resonators for Label-free Biosensing

Stephen T. Hsieh[a], Joseph E. Cheeney[a], Xi Ding[b], Nosang V. Myung[c], Elaine D. Haberer[a,b*]

[a]Materials Science and Engineering Program, University of California, Riverside, CA USA.

[b]Department of Electrical and Computer Engineering, University of California, Riverside, CA USA.

[c]Department of Chemical and Biomolecular Engineering, University of Norte Dame, Notre Dame, IN, USA.

[*]Corresponding author's e-mail: *haberer@ucr.edu*

Abstract

Whispering gallery mode (WGM) resonators have attracted attention as optical biosensors due to their capacity for rapid label-free detection. Separately, the M13 bacteriophage has been investigated as an alternative biorecognition element. In this work, a novel polymer WGM biosensor functionalized with filamentous virus biocapture agents was fabricated using near-field electrospinning (NFES) in a single step. Polyvinyl alcohol (PVA) was mixed with streptavidin-binding M13 bacteriophage and rhodamine 6G in aqueous solution for blend electrospinning of active cavity microfiber-based resonators. Confocal fluorescence microscopy revealed alignment of M13 bioreceptors along the fiber axis, while x-ray photoelectron spectroscopy (XPS) and streptavidin-conjugated nanoparticle binding studies indicated that bioactive M13 bacteriophage

were on the fiber surface. Dye-doped, crosslinked PVA/M13 fibers supported moderate quality (Q) factor first order WGM resonances within their cross-sections that exhibited a spectral shift in response to streptavidin binding. Composite PVA/M13 microfibers demonstrated specific label-free biosensing of streptavidin with a theoretical limit of detection of 3 nM and a maximum surface coverage of 21 ± 5%. These results demonstrate the potential of NFES to fabricate WGM resonators from PVA/M13 microfibers and use them as a platform for rapid, sensitive label-free sensing.

Keywords

whispering gallery mode fiber resonator, near-field electrospinning, polymer/virus composite microfiber, phage bioreceptors, label-free WGM biosensor

1. Introduction

The rapid and affordable detection of biomolecules has become a critical part of modern infrastructure. Development of sensitive and effective biosensors for biomarkers, viruses, and bacteria enables routine biomedical diagnostics, environmental monitoring, and food/water quality control. One interesting class of devices, label-free optical biosensors, targets chemical and biological agents without the need for additional fluorescent or radioactive tags, thus offering on-site and real-time detection of analytes[1]. These optical devices can also operate in harsh environments as they are not vulnerable to electromagnetic interference. In recent years, whispering gallery mode- (WGM-) based biosensors, a type of label-free optical biosensor, have shown promise due to their compact size, high sensitivity[2], and fast response time (*i.e.,* tens of seconds)[3]. Light is confined by total internal reflection at the periphery of these curved boundary high quality (Q) factor resonators and recirculates; acting as an optical probe capable of detecting minute concentrations of biomolecules. This promising technology has led to development of WGM sensors able to detect cancer biomarkers[4], bacteria[5], pesticides[6] and water contaminants[7].

Silica glass or other silicon-based compounds (*e.g.* silicon, silica, silicon nitride)[1,8–15] and polymers[16–19] are the most widely used materials for WGM optical biosensors. Because these materials lack specificity, resonators must be functionalized to recognize target analytes[4,20–24]. Device performance and manufacturability depend on the selection of both an effective biocapture agent and immobilization strategy. Bioreceptor efficacy is determined by surface density, orientation, and stability, among other factors. Antibodies, enzymes, and oligonucleotides are common biorecognition elements[25,26]. Unfortunately, these fragile biomolecules are vulnerable to extreme environments, and often have limited binding sites that

require specific orientation to ensure functionality. Moreover, they can be expensive to produce and use, requiring mammalian cell lines, sophisticated purification techniques, and/or repeated functionalization steps to achieve high receptor density.

In recent years, filamentous bacteriophages such as the M13 have attracted the interest of a handful of researchers as alternative affinity-based[21,27–29] bioreceptors. These viruses have a large density of proteins that cover the length of the phage and can be modified with high affinity peptides to serve as biorecognition elements. The wild-type M13 phage is 880 nm long and 6.5 nm in diameter. Approximately 2700 identical copies of the major coat protein (pVIII) are displayed along its length, each serving as a potential bioreceptor. Compared to individual covalently-linked or affinity bound capture agents, the viral scaffold ensures a dense, ordered arrangement of high affinity peptides with the proper orientation for analyte binding. Known as a combinatorial phage display workhorse, these viruses are also advantageous in that they can be used to construct random libraries from which peptides or proteins with affinity for a specific analyte can be selected and used without avidity concerns. Moreover, unlike other frequently used biorecognition elements, phage are chemically and thermally robust, tolerating both acidic and basic pH and temperatures up to 70°C[30]. Phage biorecognition elements can also be rapidly and inexpensively manufactured in large quantities through infection of a bacterial host without need for animal immunization.

Complex, multi-step processes are typically required for immobilization of biocapture agents on the sensor surface. For example, for silicon-based resonators, amino-terminated silanes are paired with an appropriate crosslinking chemistry to achieve covalent linkage of bioreceptors[31–34]. This process requires several steps including surface hydroxylation via acid dip or oxygen plasma treatment, vapor or liquid deposition of a silane layer, copious rinsing to

remove unreacted silane molecules, and finally, attachment of biocapture agents using carbodiimide chemistry or other bifunctional crosslinking molecule[32,33,35]. Regrettably, these additional steps, beyond cavity formation, add to device fabrication costs and complexity. One simple approach to functionalization that has been used for ampere- and potentio- metric biosensors[36,37], but not yet for WGM optical biosensors, is blend electrospinning. This rapid, low-cost manufacturing method combines biorecognition elements with a polymer solution, and then uses a strong applied electric field to draw the fluid into fibers. Biosensors are fabricated and functionalized in a single step. No post-processing is required. While electrospun electrochemical biosensors have primarily used fibers a few hundred nanometers in diameter or smaller, the fabrication technique is also capable of producing larger diameter fibers on the order of tens of microns. Indeed, recent studies have demonstrated electrospun fibers capable of supporting WGM resonances[38,39], presenting an opportunity for a one-step approach to the fabrication and functionalization of WGM optical biosensors.

This study examined near-field electrospun (NFES) polyvinyl alcohol (PVA) WGM optical biosensors with incorporated M13 bacteriophage bioreceptors (Fig. 1). Streptavidin-binding phage and rhodamine 6G were used, respectively, as a model virus-based biocapture agent and a source of high yield fluorescence. Blend electrospinning of polymer, emitter, and bioreceptor was used to achieve active cavity formation and functionalization in one step. The elimination of subsequent immobilization processes reduced fabrication complexity. Suspended, featureless fibers with circular cross-sections and an average diameter of approximately 14 μm were written over trenches on pre-patterned substrates and highly crosslinked to ensure stability in aqueous solutions and prevent swelling. Despite uniform surface appearance, confocal microscopy of fluorescently labeled phage revealed large, elongated bundles of bioreceptors

aligned to the fiber axis. These large assemblies were attributed to the reduction of M13 depletion volume caused by the PVA polymer matrix. X-ray photoelectrospectroscopy (XPS) and incubation with streptavidin-coated Au nanoparticles determined that the streptavidin-binding bacteriophage were present on the fiber surface and retained affinity. This was an important finding as the specificity of a biosensor for its target analyte depends on both the availability and functionality of biocapture agents. Emission from these optically active resonators submerged in buffer was composed of a broad fluorescent background decorated with pairs of sharp peaks with moderate Q values. Using both free spectral range and a Mie-theory derived asymptotic approximation, the peaks were identified as TE and TM whispering gallery modes supported within the electrospun fiber cross-section. Electrospun PVA/M13 fibers were employed as label-free optical biosensors for streptavidin. WGMs exhibited a red-shift in the presence of streptavidin that was not observed without the incorporation of streptavidin-binding M13 bacteriophage, indicating that the viral capture agents conferred specificity to the resonators. The theoretical lower limit of detection (LoD) was estimated to be 3 nM and a maximum streptavidin surface coverage near 21 ± 5% was calculated. The success of blend electrospinning, a potentially low-cost, large-scale manufacturing technique, in simultaneously generating and functionalizing micron-sized fibers that support WGMs and are highly sensitive to a protein analyte is an important step toward the scalable production of affordable label-free optical biosensors. This outcome is further supported by the concomitant use of the M13 filamentous virus, a combinatorial phage display workhorse and robust, inexpensive biocapture agent.

2. Material and methods

2.1 Modification and amplification of M13 filamentous virus bioreceptors

Using a previously reported protocol[28,40,41], a M13 bacteriophage was genetically modified for use as a bioreceptor in electrospun WGM optical biosensors. This virus-based biorecognition element displayed a streptavidin-binding peptide motif (VPEGAFSS)[28] on the N-terminus of each major coat protein along its length. The modified phage was amplified and purified as previously described[41]. The final stock solution was suspended in 0.1X phosphate buffer saline (PBS, 13.7 mM NaCl, 0.27 mM KCl, 1 mM Na_2HPO_4, 0.18 mM KH_2PO_4) at 1 mg/ml and stored at 4°C.

2.2 Preparation of PVA/M13 electrospinning solutions

Polymer electrospinning solutions (27% w/w) were prepared by mixing polyvinyl alcohol (PVA, 13,000-23,000 g/mol, 98% hydrolyzed, Sigma Aldrich) and deionized water. Each solution was stirred for 2 h at 80°C until the PVA was fully dissolved. After cooling for 30 min, a volume of streptavidin-binding M13 bacteriophage suspended in 0.1X PBS was added to create a PVA/M13 solution of 25% w/w PVA and 0.1 mg/ml virus. For direct comparison, a solution of 25% w/w PVA was also made by adding 0.1X PBS alone. Prior to electrospinning, ultraviolet–visible (UV-Vis) spectroscopy (ThermoFisher, Evolution 60) was used to evaluate the turbidity of the PVA/M13 and PVA solutions. A fluorescent dye, rhodamine 6G (R6G, Sigma Aldrich), was incorporated into polymer solutions at a concentration of 0.0117 mg/ml to serve as an optical emitter for active resonant biosensors.

2.3 NFES and glutaraldehyde crosslinking of PVA/M13 fibers

Square glass substrates, 15 x 15 x 1 mm, with several parallel trenches scribed in them were used for near-field electrospinning (NFES). Prior to electrospinning, the substrates were sequentially immersed and sonicated (FS20 Ultrasonic Cleaner, Fisher Scientific) in acetone, isopropanol and deionized water for 30 min to clean the surface. The substrates were then placed on a programmable X-Y stage (A-LSQ300D, Zaber). A point-plate NFES configuration (Fig. 1) with a separation of 1.25 mm between the needle tip and substrate was used to fabricate micron-scale fibers from the prepared dye-doped PVA/M13 and PVA solutions. Each polymer solution was loaded into a syringe with an attached stainless steel 27-gauge blunt-tip needle (Fisnar). A syringe pump (NE 300 US, New Era Syringe Pump) was used to flow electrospinning solution at a rate of 10 µL/h. Electrospinning was initiated by applying a 2-kV voltage between the needle and stage. As the solution was electrospun, the computer programmed X-Y stage moved 0.5 mm/s in a parallel-line pattern to produce fibers approximately 1 cm long, spaced 200 µm apart. Fibers were written perpendicular to the trenches scribed into the glass substrate to allow them to be suspended. To prevent electrospun PVA/M13 and PVA fibers from dissolving in the aqueous sensing environment, they were crosslinked using glutaraldehyde (GA, Fisher Scientific) with hydrogen chloride (HCl) as a catalyst[39]. Fibers were placed in a closed chamber and exposed to vapor from a 50% w/w GA solution and 1 M HCl for 24 h, followed by a second vapor treatment step with 50% w/w GA solution and 5 M HCl for 24 h. In the final crosslinking step, the fibers were soaked in 50% w/w GA solution for 24 h, rinsed with deionized water to remove excess GA, and dried in a vacuum desiccator for further use.

2.4 Characterization of NFES PVA/M13 fibers

Composite PVA/M13 fiber diameters were measured post-crosslinking using a digital optical microscope (KH-7700, Hirox) and associated measurement software. Fiber morphology was imaged using scanning electron microscopy (SEM; Vega3,Tescan) with an accelerating voltage of 5 kV. X-ray photoelectron spectroscopy (XPS; AXIS ULTRA^{DLD}, Kratos Analytical) was used to detect the presence of the streptavidin-binding filamentous virus bioreceptors near the fiber surface. Using an Al Kα X-ray-source, survey and high-resolution spectra were collected using pass energies of 80 and 20 eV, respectively. The functionality of the streptavidin-binding phage on the fiber surface was evaluated using streptavidin-conjugated Au nanoparticles. Streptavidin-coated Au nanoparticles (50 nm dia., Cytodiagnostics; 0.175 nM) were incubated with crosslinked PVA/M13 fibers for 3 h. The fibers were then rinsed three times with water, dried 24 h, and imaged with SEM. The areal density of bound Au nanoparticles was determined by counting the number of particles on the fiber surface and dividing by the area. The experiment was repeated three times for both PVA/M13 and PVA fibers.

Confocal fluorescence microscopy (Lecia SP5) was used to characterize the distribution of filamentous virus bioreceptors within the polymer/virus fibers. For these studies, prior to incorporation in PVA/M13 fibers, streptavidin-binding M13 bacteriophage were tagged with a fluorescent dye using a NHS-amine reactive process (DyLight™ 550 NHS Ester, Thermo Scientific). The fibers containing M13 bacteriophage bioreceptors were imaged under 543 nm laser excitation. Dye fluorescence indicated the location of the M13 virus bioreceptors. Images were analyzed using image processing software (ImageJ). The length, width, and directionality of the M13 aggregates were measured on three fibers from three separate experiments.

2.5 Excitation of WGMs and real time detection of streptavidin

WGMs were excited in the PVA/M13 and PVA fibers with a far-field laser confocal system (LabRam, Horiba Scientific), as described in a previous report[39]. A 532 nm continuous wave (CW) laser (Ventus, Laser Quantum) was focused through a 50x objective (NA = 0.75), resulting in a spot size of approximately 3 μm and an incident laser power of 6 μW. The same objective was used to collect R6G fluorescence. The collected light was directed through a long pass filter (>532 nm) into a spectrometer with a 1800 lines/mm diffraction grating and a charge-coupled device (CCD) detector. A fluorescence spectrum with spectral resolution of 0.014 nm was obtained. In all experiments, the fibers were first submerged in a 1X PBS (137 mM NaCl, 2.7 mM KCl, 10 mM Na_2HPO_4, 1.8 mM KH_2PO_4) bath for at least 24 h to eliminate any signal attributable to swelling, then transferred to a fresh 1X PBS bath to obtain spectra. Emission was recorded at 3 min intervals. To prevent photothermal effects and minimize bleaching, optical devices were not illuminated with laser light between measurements.

For analysis, the broad fluorescence background was subtracted and resonance modes were fit with Lorentzian functions to determine peak position and width. Theoretical WGM peak positions were calculated using a Mie-theory approximation[42,43]:

$$\lambda \cong \pi n_{res} D \left[\nu + \frac{\alpha_s \nu^{\frac{1}{3}}}{2^{\frac{1}{3}}} - \frac{P}{(m^2-1)^{\frac{1}{2}}} + \frac{3}{10} \frac{\alpha_s{}^2}{2^{\frac{2}{3}} \nu^{\frac{1}{3}}} - \frac{P\left(m^2 - \frac{2P}{3}\right)}{(m^2-1)^{\frac{3}{2}}} \frac{\alpha_s}{2^{\frac{1}{3}} \nu^{\frac{2}{3}}} \right]^{-1} \quad (1)$$

where D is the optically measured fiber diameter, ν is the angular mode number (l) plus 0.5, α_s are the roots of the Airy function, and n_{res} is the refractive index of the resonator. The term m is the ratio of the refractive index of the resonator to the refractive index of the surrounding medium (n_{res}/n_{surr}). P is 1/m for TM modes and m for TE modes. Here, modes with the electric

field vector perpendicular to the resonator surface are transverse magnetic (TM) and modes with the electric field vector parallel to the length of the fiber are transverse electric (TE). Computed solutions were compared to fluorescence spectra obtained from the electrospun fibers, and the least mean residual squared was taken as the best fit.

To assess the effectiveness of PVA/M13 electrospun fibers as label-free optical biosensors, the devices were placed in 1X PBS and allowed to equilibriate. Bovine serum albumin (BSA, 1 mg/mL) was added to the PBS solution as a blocking agent. Subsequently, the fibers were exposed to solutions of streptavidin (36, 218, 582, 1310 nM). Biosensing device response was measured for three PVA/M13 and three PVA electrospun fiber resonators. Spectra taken within 30 min of the addition of BSA and 10 min of streptavidin addition were excluded from device analysis to avoid transients associated with surface binding.

3. Results and discussion

3.1 Fabrication and characterization of electrospun PVA/M13 fibers

PVA fibers with incorporated M13 bacteriophage bioreceptors were fabricated using NFES. Electrospinning of water-soluble polymers such as PVA is well-suited for including large biological elements because it does not require the high temperatures, nor the harsh solvents sometimes associated with other fiber processing techniques[44,45]. In addition, the shape and form of electrospun fibers are complementary to the high aspect ratio geometry of this filamentous virus biocapture agent. By reducing the tip-to-collector distance, NFES avoids the jet instabilities and whipping associated with far-field electrospinning, resulting in a precise and controlled direct-write process. To form a composite polymer/virus solution for spinning, genetically modified M13 filamentous viruses with an affinity for streptavidin were added in low

concentration (0.1 mg/mL) to an aqueous solution of moderate molecular weight PVA (13,000-23,000 g/ml). While PVA solutions were initially transparent, they became cloudy with the addition of the virus. As shown in Fig. 2, the transmission of PVA/M13 solution was uniformly reduced throughout the entire visible range (400-900 nm), falling from 100% to 71% at 600 nm. It is important to note that the M13 bacteriophage does not absorb light at these wavelengths. The transition from optically transparent to translucent was attributed to the scattering of visible light by M13 aggregates and will be discussed later.

The polymer/virus mixture was pumped through a needle, and a droplet was generated[39]. Under an applied voltage, the droplet formed a Taylor cone, and parallel PVA/M13 fibers were deposited on a glass substrate using direct-write near-field electrospinning. Critically, the substrate was scribed with trenches prior to writing. In this way, fibers were suspended and isolated from the underlying glass, precluding optical coupling. A previously developed glutaraldehyde crosslinking process[39] was used to treat the PVA/M13 fibers and render them insoluble in aqueous solution. Glutaraldehyde formed chemical bonds between PVA polymer chains resulting in fibers that were water-stable for a minimum of 24 h[39]. As shown in Fig. 3, the near-field electrospinning process created a broad size distribution of PVA/M13 microfibers with an average diameter of 14.3 ± 5.3 μm. A representative SEM image of a crosslinked suspended composite polymer/virus fiber is also shown in Fig. 3. The surface of the suspended fibers was featureless, and no sagging was observed over scribed trenches. For comparison, using the same electrospinning conditions, microfibers were also fabricated using PVA solution without the addition of M13 bacteriophage bioreceptors (Fig. S1). Despite the disparity in solution optical properties, no significant difference was observed in appearance or size of the PVA/M13 and PVA fibers.

The homogeneity of phage-based bioreceptors within the near-field electrospun fibers was investigated using confocal fluorescence microscopy. This was of particular interest given the scattering of visible light observed when M13 phage was added to the PVA electrospinning solution. M13 biorecognition elements were fluorescently labeled (*i.e.,* Dylight 550) prior to mixing with PVA solution, then electrospun. A sample bright field microscopy image with overlaid confocal fluorescence emission is shown in Fig. 4. As shown in the figure, the fluorescence of these PVA/M13 fibers was non-uniform. The tagged M13 bacteriophage formed large oblong bundles or aggregates with an average size of 5.2 x 3.2 µm. Interactions between the virus and PVA likely produced these aggregates. Based on a report by Li *et al.*, when mixed with the polymer methylcellulose, rod-like viruses such as M13 and tobacco mosaic virus (TMV) generate large assemblies[46]. The degree of ordering within these assemblies is controlled by competing mechanisms: free volume entropy and depletion volume. In particular, in concentrated polymer solutions that have not been optimized for dispersion, the drive to reduce depletion volume can cause M13 to bundle. Of course, with respect to device reliability and repeatability, a uniform distribution of bioreceptors on the sensor surface is more desirable than randomly positioned assemblies. More studies are needed to tune attractive and repulsive forces through polymer concentration, phage concentration, and ionic strength in order to minimize M13 aggregation. The phage aggregates were oriented with a directionality of 1.0° with respect to the fiber axis (Fig. 4). In contrast, phage aggregates formed in dropcast films showed no directionality (Fig. S2). The alignment of biological materials within electrospun polymers has been previously observed for high aspect, rod-like particles including TMV, M13, and *E. coli*. [44,47,48]. The sink-like flow in the Taylor cone causes mechanical stresses that orient the biological elements[48]. With further development, it may be possible to control both the

packing density and alignment of the M13. Long-range ordering and high surface coverage of bioreceptors would be an asset for electrospun fiber biosensor design.

For a biorecognition element to impart specificity to a sensor, it must be both accessible and functional. Only biorecognition elements on the fiber surface contribute to analyte binding and detection. The presence of bioreceptors on the surface of the composite PVA/M13 fibers was assessed using XPS. While the DNA and proteins that comprise M13 bacteriophage contain nitrogen, PVA does not. This compositional difference was exploited to identify exposed biorecognition elements. Similar strategies have been used to identify core-shell electrospun fibers, as well as the presence of proteins or polyelectrolytes on the surface of electrospun fibers[49–51]. As shown in Fig. 5, peaks with binding energies of 400 and 404 eV were observed and attributed to nitrogen. In contrast, electrospun PVA fibers had no discernable peaks at these energies. The observation of nitrogen indicated that a measurable amount of M13 added to the electrospinning solution was located on the PVA/M13 fiber surface. Nanoparticle conjugates were used to study the streptavidin binding activity of the bioreceptors on the fiber exterior. Following crosslinking, PVA/M13 fibers were incubated with a low concentration of streptavidin-coated Au nanoparticles, thoroughly rinsed, and imaged. Electrospun PVA fibers were also prepared and imaged in the same manner. A representative electron microscopy image of a PVA/M13 fiber with bound Au nanoparticles is shown in Fig. 6. The surface density of Au nanoparticles was tallied for each type of fiber and displayed in Fig. 6. The addition of streptavidin-binding phage increased the conjugated particle density by approximately 22% over PVA fibers alone. The up-tick in binding phage signaled retention of bioreceptor functionality throughout the fiber fabrication process, including both electrospinning and crosslinking steps.

3.2 Excitation of WGM resonance in PVA/M13 fibers

The optical performance of the electrospun polymer/virus WGM fiber resonators was evaluated. A broad spectrum emitter, R6G, was added to the electrospinning solution during the mixing process, transforming the fiber into an active resonator. Embedded emitters allowed the use of free-space optics for excitation and collection of WGMs. The dye-doped electrospun fiber resonators were placed in 1X PBS[52]. Because this isotonic buffer has an ionic strength and osmolarity comparable to the human body, it is commonly used in biological research, including biosensor experiments. A 532 nm continuous wave (CW) laser with 6 μW of power was focused through a microscope objective and used to excite the resonators. Emission was collected through the same objective and spectrally analyzed. In contrast to near-field optical coupling approaches such as fibers or prisms, free-space coupling spatially separates measurement optics from the analyte, preventing unwanted interactions. Furthermore, free-space optics can reduce mechanical noise because they are less susceptible to positional changes during measurement and increase portability because they are compatible with light emitting diode excitation [24,53] and on-chip microfluidic integration [54,55]. Fig. 7 shows a representative spectrum from a dye-doped, crosslinked PVA/M13 fiber with a 18.7 μm diameter, as measured optically. The broad emitter fluorescence background of the active electrospun fiber cavity was subtracted to highlight the resonant modes. The sharp, regularly spaced peaks were ascribed to WGMs supported by the circular cross-section of the fiber and dictated by the resonance condition

$$l\lambda = \pi D n_{res} \quad (2)$$

where *l* is a positive integer indicating the angular mode number, λ is the wavelength, D is the resonator diameter, and n_{res} is the refractive index of the resonator. Resonant peaks appeared in pairs with a free spectral range (FSR) or spacing between consecutive mode pairs of 4.382 nm. Notably, each peak had a high-energy shoulder attributable to the spiral or conical modes that often develop in cylindrical WGM resonators. These modes exist due to higher-order axial modes with similar angular mode numbers that are non-degenerate due to the non-spheroidal cavity geometry[56–60]. Although the shoulder could represent a convolution of innumerable closely spaced modes, a simple two Lorentzian fit was used to analyze the asymmetric peaks as shown in Fig. 7. As an example, a central wavelength of 598.035 nm and Q value of 2367 were found for this high-quality WGM resonance. Empirical WGM peak positions were compared to those computed using a Mie-theory derived approximation[42,43]. The observed high-quality peaks were identified as first-order radial WGMs. Mode assignments, shown in Fig. 7, correspond to a fiber diameter of 18.4 μm and n_{res} of 1.464[39] and are consistent with previously measured values[39]. The shorter wavelength peak within a pair was a TM mode, whereas the longer wavelength peak was a TE mode. Notably, the TE modes were consistently higher in Q and intensity. For this reason, they were selected for use in biosensing studies.

3.3 Label-free detection of streptavidin with electrospun PVA/M13 fiber WGM resonators

Blend electrospun PVA/M13 fibers had both functional virus bioreceptors with an affinity for streptavidin on their surface and supported WGM resonances within their cross-section. These readily manufacturable, polymer-based resonators were assessed as label-free optical biosensors for streptavidin. The sensitivity of a WGM sensor is tied to the magnitude of the evanescent field at the resonator surface, and can vary with resonator size and quality [61,62]. For optical mode

uniformity, polymer/virus fiber resonators with diameters between 17 and 22 μm, and Q values between 1350 and 4000 were selected for measurement. In addition, PVA fiber resonators with the same specifications were also chosen to aid in evaluation of M13 bioreceptor performance. The resonance of each fiber-based device was recorded in PBS for a minimum of 50 min prior to biosensing experiments. No trends were observed in spectral peak position during this time (Fig. S3), thus indicating a mechanically unchanging PVA/M13 fiber and stable M13 bioreceptor surface density. Following this initial stabilization period, BSA was added to the PBS solution to limit non-specific binding contributions. BSA is regularly used as a blocking agent for a variety of biosensors and is compatible with phage-based bioreceptors and WGM optical resonators[4,21,29,63]. A spectral line shift was observed with the addition of BSA and, again, the system was allowed to achieve equilibrium (Fig. S3). The average resonance wavelength in BSA was used as the reference point for spectral shifts associated with streptavidin binding. The spectral resolution of the system was found using the standard deviation of the resonance peak in BSA, $\sigma = 0.008$ nm.

The blocked electrospun fiber biosensors were exposed to streptavidin concentrations ranging from 36 to 1310 nM. A representative spectral shift observed for a PVA/M13 electrospun fiber device at the highest streptavidin concentration is shown in Fig. 8. With the addition of 1310 nM streptavidin, an average red-shift of 0.063 ± 0.016 nm was observed. Biomolecules, such as streptavidin, typically have a higher polarizability than the surrounding medium. Upon binding to the cavity surface, interactions with the WGM evanescent field cause an increase in resonance wavelength. Markedly, a comparable spectral shift was not observed for PVA fibers indicating that the M13 virus bioreceptors promoted streptavidin-specific binding on the cavity surface. In Fig. 8, the average spectral responses of the electrospun resonators are

shown as a function of streptavidin concentration for both PVA/M13 and PVA electrospun WGM resonators. Differences in PVA/M13 electrospun resonator diameter and non-uniform bioreceptor distribution likely contributed to variation in spectral response. The relationship between the resonant peak of the polymer/virus fibers and streptavidin concentration was fit using the Hill model ($R^2 = 0.914$). The sensitivity (S) of the linear region (0 to 36 nM) was 0.008 nm/nM. The theoretical limit of detection (LoD) or the smallest resolvable response was estimated as $LoD = 3\sigma/S = 3$ nM. For comparison, dye-doped poly-methyl methacrylate microdisk lasers and polystyrene microsphere lasers have achieved theoretical detection limits of 104 ng/ml (2 nM) for streptavidin[54] and 4 nM for neutravidin[64], respectively, using the interaction with biotin as a model high-affinity system. While these polymer-based active WGM resonators had similar limits of detection, unlike the electrospun fiber WGM biosensor, they required additional functionalization steps following cavity formation. Notably, despite the usefulness of biotin as a model bioreceptor, biotin exhibits quite a bit of promiscuity, binding indiscriminately with the majority of avidin-like molecules. In contrast, through the combinatorial phage display process, the M13 phage-based bioreceptor has the potential to discriminate among streptavidin, avidin, and neutravidin[28] .

The surface density of streptavidin bound to composite PVA/M13 fiber biosensors can be estimated using the response of the WGM resonator. Assuming a single layer of randomly bound biomolecules and summing over the entire surface of the resonator leads to the equation[65,66]

$$\frac{\Delta\lambda}{\lambda} = \frac{\alpha_{ex}\sigma_p}{\epsilon_0({n_{res}}^2 - {n_{surr}}^2)R} \quad (3)$$

Where α_{ex} is the excess polarizability of streptavidin ($4\pi\varepsilon_0 \cdot 3.85 \times 10^{-21}$) cm^3[66], R is the radius of the resonator, n_{res} is the index of refraction of the PVA fiber (1.464)[39], and n_{surr} is the index of refraction of the surrounding PBS (1.3338), and σ_p is the surface density of the bound streptavidin. Assuming streptavidin is a 5 nm sphere and a square close-packed monolayer, the maximal surface density of streptavidin is 4×10^{12} streptavidin/cm^2 [67]. For the PVA/M13 devices in 1310 nM of streptavidin, we determined a surface density of $8.5 \times 10^{11} \pm 2.1 \times 10^{11}$ streptavidin/cm^2 which is equivalent to 21 ± 5% coverage of the PVA/M13 fiber surface (Fig. S4). Assuming the streptavidin surface coverage approximately corresponds to that of the streptavidin-binding phage, the percentage of surface area covered with bioreceptors is comparable to that observed for other M13-based optical resonator biosensors[21]. Nonetheless, the relatively low coverage indicates a possible avenue of sensor improvement. Future studies will focus on raising the sensitivity and lowering the detection limit of electrospun WGM biosensors by increasing the density and uniformity of M13 filamentous virus bioreceptors on the fiber surface.

4. Conclusion

Blend NFES of PVA and M13 filamentous bacteriophage is a simple strategy for immobilization of biocapture agents on WGM optical cavities. In a single step, both optical cavity formation and functionalization were achieved. Resonant wavelength shifts were tracked with the addition of a protein analyte. Specific binding of streptavidin to the resonator was observed with a sensitivity of 0.008 nm/nM and a LoD of 3 nM. Despite bioreceptor aggregation and relatively low analyte surface coverage (21%), sensor performance was comparable to reports[54,64] for other polymer-based active WGM optical biosensors that used more complex, multi-step

immobilization processes and less robust biocapture agents. These results warrant further investigation of this scalable, low-cost sensing platform with emphasis on tuning bioreceptor dispersion and surface coverage. The wedding of the M13, a combinatorial phage display mainstay, with a rapid, inexpensive optical cavity manufacturing approach presents a versatile sensing platform with the potential to detect a broad range of analytes.

Acknowledgements

This material is based upon work supported by the National Science Foundation under Grant No. ECCS-1406795. Additional support was provided by the UCR CoR Grant Program. S.T.H. is grateful for support from the U. S. Department of Education via the Graduate Assistance in Areas of National Need program. In addition, this study utilized the Analytical Chemistry Instrumentation Facility, the Institute for Integrative Genome Biology, and Central Facility for Advanced Microscopy and Microanalysis at University of California, Riverside.

References

[1] F. Vollmer, S. Arnold, Whispering-gallery-mode biosensing: Label-free detection down to single molecules, Nat. Methods. 5 (2008) 591–596. https://doi.org/10.1038/nmeth.1221.

[2] V.R. Dantham, S. Holler, C. Barbre, D. Keng, V. Kolchenko, S. Arnold, Label-free detection of single protein using a nanoplasmonic-photonic hybrid microcavity, Nano Lett. 13 (2013) 3347–3351. https://doi.org/10.1021/nl401633y.

[3] J. Su, Label-Free biological and chemical sensing using whispering gallery mode optical resonators: Past, present, and future, Sensors (Switzerland). 17 (2017) 1–18. https://doi.org/10.3390/s17030540.

[4] H.A. Huckabay, S.M. Wildgen, R.C. Dunn, Label-free detection of ovarian cancer biomarkers using whispering gallery mode imaging, Biosens. Bioelectron. 45 (2013) 223–229. https://doi.org/10.1016/j.bios.2013.01.072.

[5] H. Ghali, H. Chibli, J.L. Nadeau, P. Bianucci, Y.A. Peter, Real-time detection of Staphylococcus aureus using Whispering Gallery Mode optical microdisks, Biosensors. 6 (2016) 1–9. https://doi.org/10.3390/bios6020020.

[6] R. Duan, X. Hao, Y. Li, H. Li, Detection of acetylcholinesterase and its inhibitors by liquid crystal biosensor based on whispering gallery mode, Sensors Actuators, B Chem. 308 (2020) 127672. https://doi.org/10.1016/j.snb.2020.127672.

[7] S. Berneschi, F. Bettazzi, A. Giannetti, F. Baldini, G. Nunzi, S. Pelli, I. Palchetti, Trends in Analytical Chemistry Optical whispering gallery mode resonators for label-free detection of water contaminants, Trends Anal. Chem. 126 (2020) 115856. https://doi.org/10.1016/j.trac.2020.115856.

[8] M. Pöllinger, D. O'Shea, F. Warken, A. Rauschenbeutel, Ultrahigh-Q tunable whispering-

gallery-mode microresonator., Phys. Rev. Lett. 103 (2009) 1–4. https://doi.org/10.1103/PhysRevLett.103.053901.

[9] D. Navarro-Urrios, M. Baselga, F.F. Lupi, L.L. Martín, C. Pérez-Rodríguez, V. Lavin, I.R. Martín, B. Garrido, N.E. Capuj, Local characterization of rare-earth-doped single microspheres by combined microtransmission and microphotoluminescence techniques, J. Opt. Soc. Am. B. 29 (2012) 3293–3298. https://doi.org/10.1364/josab.29.003293.

[10] S. Imamura, R. Watahiki, R. Miura, T. Shimada, Y.K. Kato, Optical control of individual carbon nanotube light emitters by spectral double resonance in silicon microdisk resonators, Appl. Phys. Lett. 102 (2013) 161102. https://doi.org/10.1063/1.4802930.

[11] B.D. Jones, M. Oxborrow, V.N. Astratov, M. Hopkinson, A. Tahraoui, M.S. Skolnick, A.M. Fox, Splitting and lasing of whispering gallery modes in quantum dot micropillars, Opt. InfoBase Conf. Pap. 18 (2011) 3302–3307. https://doi.org/10.1364/oe.18.022578.

[12] S.L. McCall, A.F.J. Levi, R.E. Slusher, S.J. Pearton, R.A. Logan, Whispering-gallery mode microdisk lasers, Appl. Phys. Lett. 60 (1992) 289–291. https://doi.org/10.1063/1.106688.

[13] E.D. Haberer, R. Sharma, C. Meier, A.R. Stonas, S. Nakamura, S.P. Denbaars, E.L. Hu, Free-standing, optically pumped, GaN/InGaN microdisk lasers fabricated by photoelectrochemical etching, Appl. Phys. Lett. 85 (2004) 5179–5181. https://doi.org/10.1063/1.1829167.

[14] T. Kipp, H. Welsch, C. Strelow, C. Heyn, D. Heitmann, Optical modes in semiconductor microtube ring resonators., Phys. Rev. Lett. 96 (2006) 077403. https://doi.org/10.1103/PhysRevLett.96.077403.

[15] K. Srinivasan, A. Stintz, S. Krishna, O. Painter, Photoluminescence measurements of

quantum-dot-containing semiconductor microdisk resonators using optical fiber taper waveguides, Phys. Rev. B - Condens. Matter Mater. Phys. 72 (2005) 205318. https://doi.org/10.1103/PhysRevB.72.205318.

[16] T. Grossmann, S. Schleede, M. Hauser, M.B. Christiansen, C. Vannahme, C. Eschenbaum, S. Klinkhammer, T. Beck, J. Fuchs, G.U. Nienhaus, U. Lemmer, A. Kristensen, T. Mappes, H. Kalt, Low-threshold conical microcavity dye lasers, Appl. Phys. Lett. 97 (2010) 1–4. https://doi.org/10.1063/1.3479532.

[17] V.D. Ta, R. Chen, L. Ma, Y. Jun Ying, H.D. Sun, Whispering gallery mode microlasers and refractive index sensing based on single polymer fiber, Laser Photonics Rev. 7 (2013) 133–139. https://doi.org/10.1002/lpor.201200074.

[18] A.M. Armani, A. Srinivasan, K.J. Vahala, Soft lithographic fabrication of high Q polymer microcavity arrays, Nano Lett. 7 (2007) 1823–1826. https://doi.org/10.1021/nl0708359.

[19] A. François, N. Riesen, H. Ji, S. Afshar V., T.M. Monro, Polymer based whispering gallery mode laser for biosensing applications, Appl. Phys. Lett. 106 (2015) 031104. https://doi.org/10.1063/1.4905931.

[20] I. Brice, K. Grundsteins, A. Atvars, J. Alnis, R. Viter, A. Ramanavicius, Whispering gallery mode resonator and glucose oxidase based glucose biosensor, Sensors Actuators, B Chem. 318 (2020) 128004. https://doi.org/10.1016/j.snb.2020.128004.

[21] H. Zhu, I.M. White, J.D. Suter, X. Fan, Phage-based label-free biomolecule detection in an opto-fluidic ring resonator, Biosens. Bioelectron. 24 (2008) 461–466. https://doi.org/10.1016/j.bios.2008.04.028.

[22] G. Nunzi Conti, S. Berneschi, S. Soria, Aptasensors Based on Whispering Gallery Mode Resonators., Biosensors. 6 (2016). https://doi.org/10.3390/bios6030028.

[23] Z. Guo, Y. Qin, P. Chen, J. Hu, Y. Zhou, X. Zhao, Z. Liu, Y. Fei, X. Jiang, X. Wu, Hyperboloid-Drum Microdisk Laser Biosensors for Ultrasensitive Detection of Human IgG, Small. 16 (2020) 1–9. https://doi.org/10.1002/smll.202000239.

[24] Y. Kim, H. Lee, On-chip label-free biosensing based on active whispering gallery mode resonators pumped by a light-emitting diode, Opt. Express. 27 (2019) 34405. https://doi.org/10.1364/oe.27.034405.

[25] N. Bhalla, P. Jolly, N. Formisano, P. Estrela, Introduction to biosensors, Essays Biochem. 60 (2016) 1–8. https://doi.org/10.1042/EBC20150001.

[26] I. Bazin, S.A. Tria, A. Hayat, J.L. Marty, New biorecognition molecules in biosensors for the detection of toxins, Biosens. Bioelectron. 87 (2017) 285–298. https://doi.org/10.1016/j.bios.2016.06.083.

[27] L. Han, P. Liu, V.A. Petrenko, A.H. Liu, A label-free electrochemical impedance cytosensor based on specific peptide-fused phage selected from landscape phage library, Sci. Rep. 6 (2016) 1–10. https://doi.org/10.1038/srep22199.

[28] V.A. Petrenko, G.P. Smith, Phages from landscape libraries as substitute antibodies, Protein Eng. Des. Sel. 13 (2000) 589–592. https://doi.org/10.1093/protein/13.8.589.

[29] V. Nanduri, S. Balasubramanian, S. Sista, V.J. Vodyanoy, A.L. Simonian, Highly sensitive phage-based biosensor for the detection of β-galactosidase, Anal. Chim. Acta. 589 (2007) 166–172. https://doi.org/10.1016/j.aca.2007.02.071.

[30] C.M. Warner, N. Barker, S.W. Lee, E.J. Perkins, M13 bacteriophage production for large-scale applications, Bioprocess Biosyst. Eng. 37 (2014) 2067–2072. https://doi.org/10.1007/s00449-014-1184-7.

[31] Y. Zhang, T. Zhou, B. Han, A. Zhang, Y. Zhao, Optical bio-chemical sensors based on

whispering gallery mode resonators, Nanoscale. 10 (2018) 13832–13856. https://doi.org/10.1039/c8nr03709d.

[32] H.K. Hunt, C. Soteropulos, A.M. Armani, Bioconjugation strategies for microtoroidal optical resonators, Sensors (Switzerland). 10 (2010) 9317–9336. https://doi.org/10.3390/s101009317.

[33] M.S. Luchansky, R.C. Bailey, High-Q optical sensors for chemical and biological analysis, Anal. Chem. 84 (2012) 793–821. https://doi.org/10.1021/ac2029024.

[34] C.E. Soteropulos, K.M. Zurick, M.T. Bernards, H.K. Hunt, Tailoring the protein adsorption properties of whispering gallery mode optical biosensors, Langmuir. 28 (2012) 15743–15750. https://doi.org/10.1021/la302041d.

[35] N.B. Arnfinnsdottir, C.A. Chapman, R.C. Bailey, A. Aksnes, B.T. Stokke, Impact of silanization parameters and antibody immobilization strategy on binding capacity of photonic ring resonators, Sensors (Switzerland). 20 (2020). https://doi.org/10.3390/s20113163.

[36] N. Aliheidari, N. Aliahmad, M. Agarwal, H. Dalir, Electrospun nanofibers for label-free sensor applications, Sensors (Switzerland). 19 (2019). https://doi.org/10.3390/s19163587.

[37] G. Ren, X. Xu, Q. Liu, J. Cheng, X. Yuan, L. Wu, Y. Wan, Electrospun poly(vinyl alcohol)/glucose oxidase biocomposite membranes for biosensor applications, React. Funct. Polym. 66 (2006) 1559–1564. https://doi.org/10.1016/j.reactfunctpolym.2006.05.005.

[38] X. Chen, K. Xie, T. Hu, X. Zhang, Y. Yang, J. Ma, J. Zhang, X. Cheng, Z. Hu, Whispering gallery mode microlaser based on a single polymer fiber fabricated by electrospinning, J. Phys. D. Appl. Phys. 52 (2019) 475104. https://doi.org/10.1088/1361-

6463/ab39f1.

[39] J.E. Cheeney, S.T. Hsieh, N. V. Myung, E.D. Haberer, Whispering gallery mode emission from dye-doped polymer fiber cross-sections fabricated by near-field electrospinning, Nanoscale. 12 (2020) 9873–9883. https://doi.org/10.1039/d0nr00147c.

[40] Y. Huang, C.Y. Chiang, S.K. Lee, Y. Gao, E.L. Hu, J. De Yoreo, A.M. Belcher, Programmable assembly of nanoarchitectures using genetically engineered viruses, Nano Lett. 5 (2005) 1429–1434. https://doi.org/10.1021/nl050795d.

[41] M.S. Zaman, C.H. Moon, K.N. Bozhilov, E.D. Haberer, Phage-directed synthesis of copper sulfide: Structural and optical characterization, Nanotechnology. 24 (2013). https://doi.org/10.1088/0957-4484/24/32/325602.

[42] C.C. Lam, P.T. Leung, K. Young, Explicit asymptotic formulas for the positions, widths, and strengths of resonances in Mie scattering, J. Opt. Soc. Am. B. 9 (1992) 1585. https://doi.org/10.1364/josab.9.001585.

[43] F. Khozeymeh, M. Razaghi, Cylindrical optical resonators: Fundamental properties and bio-sensing characteristics, J. Opt. (United Kingdom). 20 (2018). https://doi.org/10.1088/2040-8986/aab052.

[44] S.W. Lee, A.M. Belcher, Virus-based fabrication of micro- and nanofibers using electrospinning, Nano Lett. 4 (2004) 387–390. https://doi.org/10.1021/nl034911t.

[45] R. Sugimoto, J.H. Lee, J.H. Lee, H.E. Jin, S.Y. Yoo, S.W. Lee, Bacteriophage nanofiber fabrication using near field electrospinning, RSC Adv. 9 (2019) 39111–39118. https://doi.org/10.1039/c9ra07510k.

[46] T. Li, X. Zan, Y. Sun, X. Zuo, X. Li, A. Senesi, R.E. Winans, Q. Wang, B. Lee, Self-assembly of rodlike virus to superlattices, Langmuir. 29 (2013) 12777–12784.

https://doi.org/10.1021/la402933q.

[47] L. Wu, J. Zang, L.A. Lee, Z. Niu, G.C. Horvatha, V. Braxtona, A.C. Wibowo, M.A. Bruckman, S. Ghoshroy, H.-C. zur Loye, X. Li, Q. Wang, Electrospinning fabrication, structural and mechanical characterization of rod-like virus-based composite nanofibers, J. Mater. Chem. 21 (2011) 8550. https://doi.org/10.1039/c1jm00078k.

[48] W. Salalha, J. Kuhn, Y. Dror, E. Zussman, Encapsulation of bacteria and viruses in electrospun nanofibres., Nanotechnology. 17 (2006) 4675–4681. https://doi.org/10.1088/0957-4484/17/18/025.

[49] S.T. Sullivan, C. Tang, A. Kennedy, S. Talwar, S.A. Khan, Electrospinning and heat treatment of whey protein nanofibers, Food Hydrocoll. 35 (2014) 36–50. https://doi.org/10.1016/j.foodhyd.2013.07.023.

[50] G. Chen, D. Fang, K. Wang, J. Nie, G. Ma, Core-shell structure PEO/CS nanofibers based on electric field induced phase separation via electrospinning and its application, J. Polym. Sci. Part A Polym. Chem. 53 (2015) 2298–2311. https://doi.org/10.1002/pola.27702.

[51] C. Tang, A.E. Ozcam, B. Stout, S.A. Khan, Effect of pH on protein distribution in electrospun PVA/BSA composite nanofibers, Biomacromolecules. 13 (2012) 1269–1278. https://doi.org/10.1021/bm2017146.

[52] M. Himmelhaus, S. Krishnamoorthy, A. Francois, Optical sensors based on whispering gallery modes in fluorescent microbeads: Response to specific interactions, Sensors. 10 (2010) 6257–6274. https://doi.org/10.3390/s100606257.

[53] B. Niu, X. Shi, K. Ge, J. Ruan, Z. Xu, S. Zhang, D. Guo, T. Zhai, An all-optical tunable polymer WGM laser pumped by a laser diode, Nanoscale Adv. (2022) 2153–2158. https://doi.org/10.1039/d2na00025c.

[54] S.F. Wondimu, M. Hippler, C. Hussal, A. Hofmann, S. Krämmer, J. Lahann, H. Kalt, W. Freude, C. Koos, Robust label-free biosensing using microdisk laser arrays with on-chip references, Opt. Express. 26 (2018) 3161. https://doi.org/10.1364/oe.26.003161.

[55] X. Ouyang, T. Liu, Y. Zhang, J. He, Z. He, A.P. Zhang, H.Y. Tam, Ultrasensitive optofluidic enzyme-linked immunosorbent assay by on-chip integrated polymer whispering-gallery-mode microlaser sensors, Lab Chip. 20 (2020) 2438–2446. https://doi.org/10.1039/d0lc00240b.

[56] V. Zamora, A. Díez, M. V. Andrés, B. Gimeno, Cylindrical optical microcavities: Basic properties and sensor applications, Photonics Nanostructures - Fundam. Appl. 9 (2011) 149–158. https://doi.org/10.1016/j.photonics.2010.09.007.

[57] M. Sumetsky, Localization of light on a cone: theoretical evidence and experimental demonstration for an optical fiber, Opt. Lett. 36 (2011) 145–147. https://doi.org/10.1364/ol.36.000145.

[58] M. Sumetsky, Optical bottle microresonators, Prog. Quantum Electron. 64 (2019) 1–30. https://doi.org/10.1016/j.pquantelec.2019.04.001.

[59] F. Luan, E. Magi, T. Gong, I. Kabakova, B.J. Eggleton, Photoinduced whispering gallery mode microcavity resonator in a chalcogenide microfiber, Opt. Lett. 36 (2011) 4761–4763. https://doi.org/10.1364/ol.36.004761.

[60] J.W. Silverstone, S. McFarlane, C.P.K. Manchee, A. Meldrum, Ultimate resolution for refractometric sensing with whispering gallery mode microcavities, Opt. Express. 20 (2012) 8284. https://doi.org/10.1364/oe.20.008284.

[61] F. Khozeymeh, M. Razaghi, Sensitivity optimization in whispering gallery mode optical cylindrical biosensors, in: J. Phys. Conf. Ser., 2018: pp. 0–6. https://doi.org/10.1088/1742-

6596/956/1/012008.

[62] T. Reynolds, M.R. Henderson, A. François, N. Riesen, J.M.M. Hall, S. V. Afshar, S.J. Nicholls, T.M. Monro, Optimization of whispering gallery resonator design for biosensing applications, Opt. Express. 23 (2015) 17067. https://doi.org/10.1364/oe.23.017067.

[63] W. Shen, S. Li, M.-K. Park, Z. Zhang, Z. Cheng, V.A. Petrenko, B.A. Chin, Blocking Agent Optimization for Nonspecific Binding on Phage Based Magnetoelastic Biosensors, J. Electrochem. Soc. 159 (2012) B818–B823. https://doi.org/10.1149/2.057210jes.

[64] A. François, T. Reynolds, T.M. Monro, A fiber-tip label-free biological sensing platform: A practical approach toward in-vivo sensing, Sensors (Switzerland). 15 (2015) 1168–1181. https://doi.org/10.3390/s150101168.

[65] Y. Wu, F. Vollmer, Whispering Gallery Mode Biomolecular Sensors, in: Springer Ser. Opt. Sci., 2014: pp. 323–349. https://doi.org/10.1007/978-3-642-40003-2.

[66] S. Arnold, M. Khoshsima, I. Teraoka, S. Holler, F. Vollmer, Shift of whispering-gallery modes in microspheres by protein adsorption, Opt. Lett. 28 (2003) 272. https://doi.org/10.1364/ol.28.000272.

[67] J.P. Landry, Y.S. Sun, X.W. Guo, X.D. Zhu, Protein reactions with surface-bound molecular targets detected by oblique-incidence reflectivity difference microscopes, Appl. Opt. 47 (2008) 3275–3288. https://doi.org/10.1364/AO.47.003275.

Figure Captions:

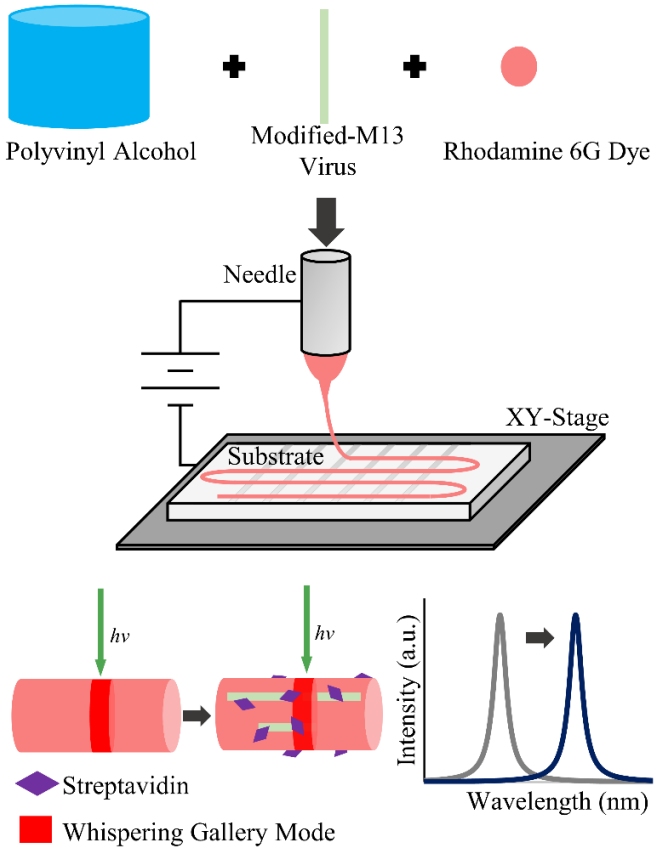

Fig. 1: Schematic of near-field electrospinning (NFES) apparatus used to form whispering gallery mode (WGM) fiber biosensors. Polyvinyl alcohol (PVA), M13 filamentous virus bioreceptors, and rhodamine 6G (R6G) are combined in solution and electrospun under an applied voltage onto a scribed substrate to form suspended fibers. Under laser excitation, fluorescence from R6G is modulated by WGMs circulating at the fiber perimeter. The binding of a target analyte to M13 bioreceptors shifts the resonance of the WGMs.

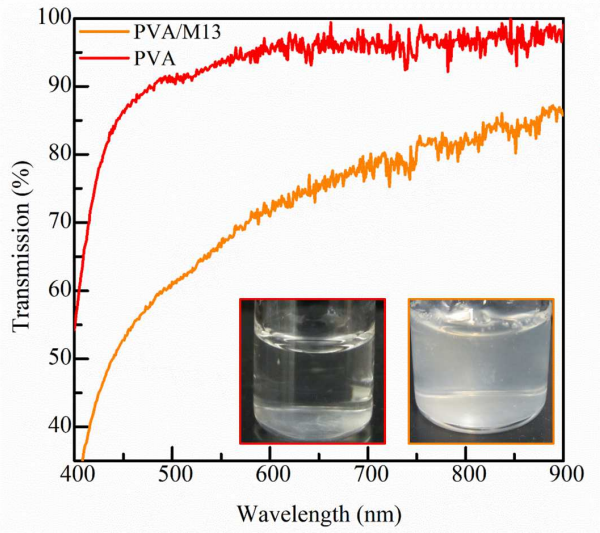

Fig. 2: Transmission spectra of PVA/M13 and PVA electrospinning solutions. Inset: Optical images of the PVA (left) and PVA/M13 (right) solutions.

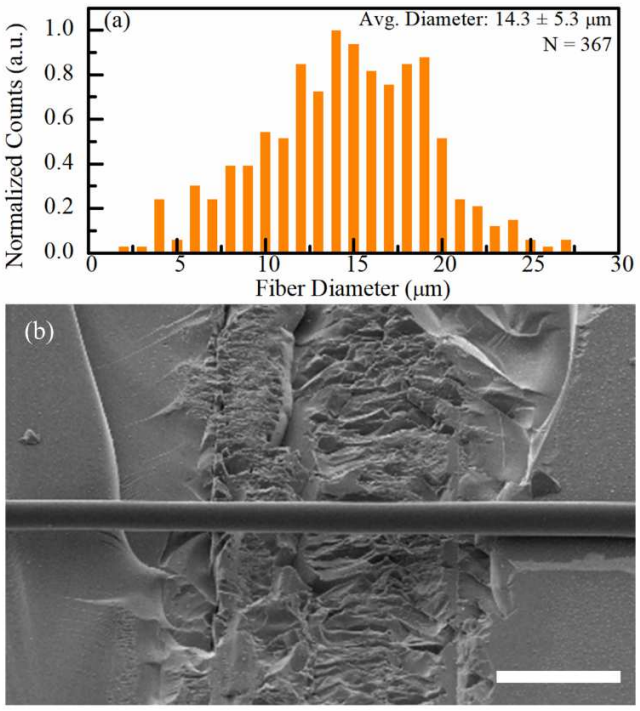

Fig. 3: a) Histogram of PVA/M13 near-field electrospun (NFES) fiber diameter. (b) Scanning electron microscopy (SEM) image of a PVA/M13 fiber suspended over a trench that has been scribed in the underlying glass substrate. Scale bar: 50 µm

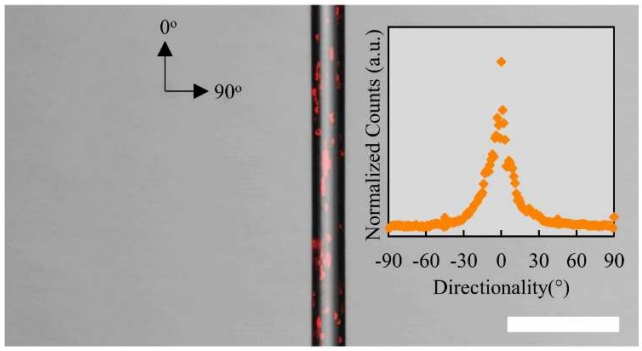

Fig. 4: A bright field image of a PVA/M13 near-field electrospun fiber with overlaid confocal fluorescence emission. The M13 bacteriophage within the fiber have been tagged with a fluorescent dye. Inset: Phage directionality that has been measured with respect to the fiber axis. Scale bar: 50 µm

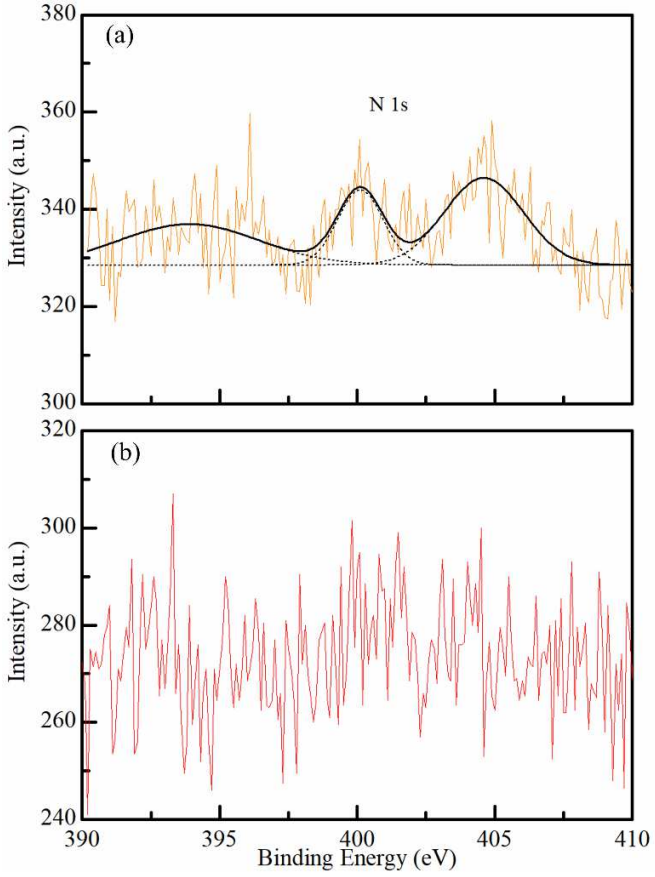

Fig. 5: X-ray photoelectron spectroscopy (XPS) spectra of the N-region of near-field electrospun (a) PVA/M13 and (b) PVA fibers with deconvolution of the N peaks.

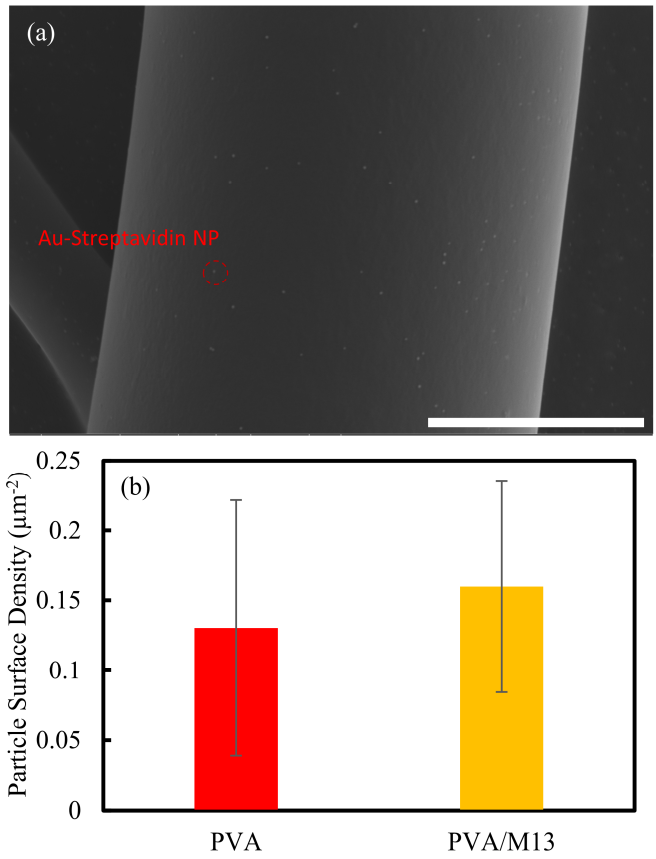

Fig. 6: a) A representative SEM image of streptavidin-coated Au nanoparticles bound to the surface of a near-field electrospun PVA/M13 fiber. b) Gold nanoparticle surface density after incubation with PVA and PVA/M13 fibers (N = 3). Scale bar: 5 µm

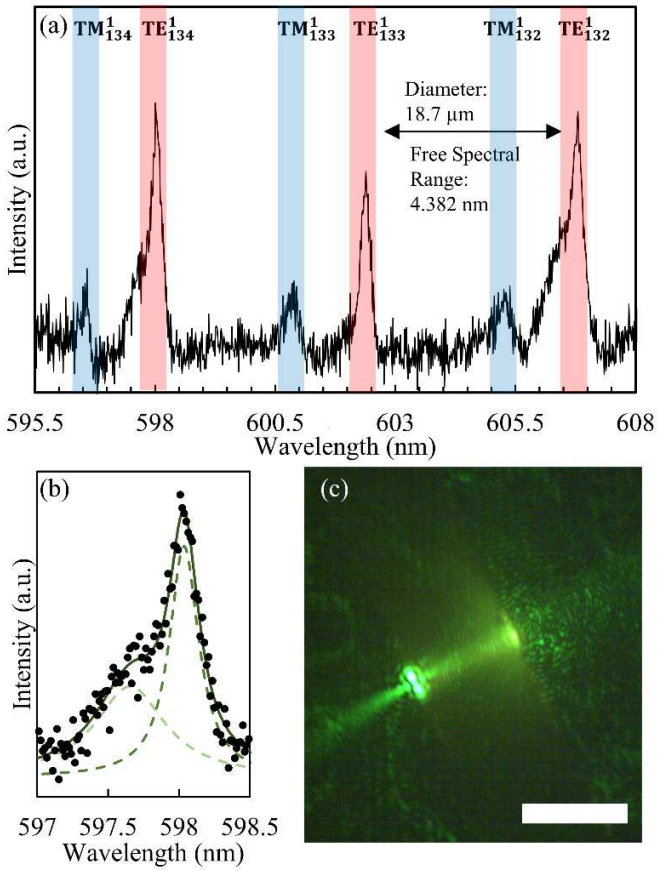

Fig. 7: (a) Photoluminescence spectrum of an 18.7 μm diameter electrospun PVA/M13 fiber measured in PBS. The broad fluorescence background was decorated by WGMs. Mie theory was used to assign radial and angular mode numbers, as well as mode polarization. (b) An individual TE mode with a two Lorentzian curve fit. A Q-factor of 2367 was obtained for the 598.035 nm peak. (c) An optical image of a 22 μm diameter electrospun fiber WGM resonator in PBS under laser illumination. Scale bar: 20 μm

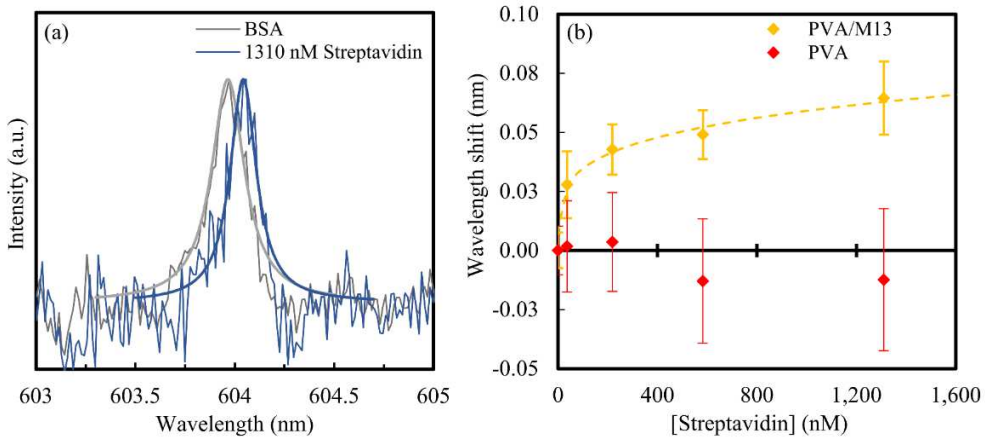

Fig. 8: (a) A WGM resonance peak of a PVA/M13 fiber submerged in BSA solution, as well as the same mode in a 1310 nM streptavidin solution. The resonance red shifted due to the specific binding of streptavidin to the resonator surface. (b) The resonant wavelength shift compared to BSA due to the addition of a range of streptavidin concentrations. The device response was collected from three PVA/M13 and three PVA devices. The data are fitted using the Hill model ($R^2 = 0.941$).

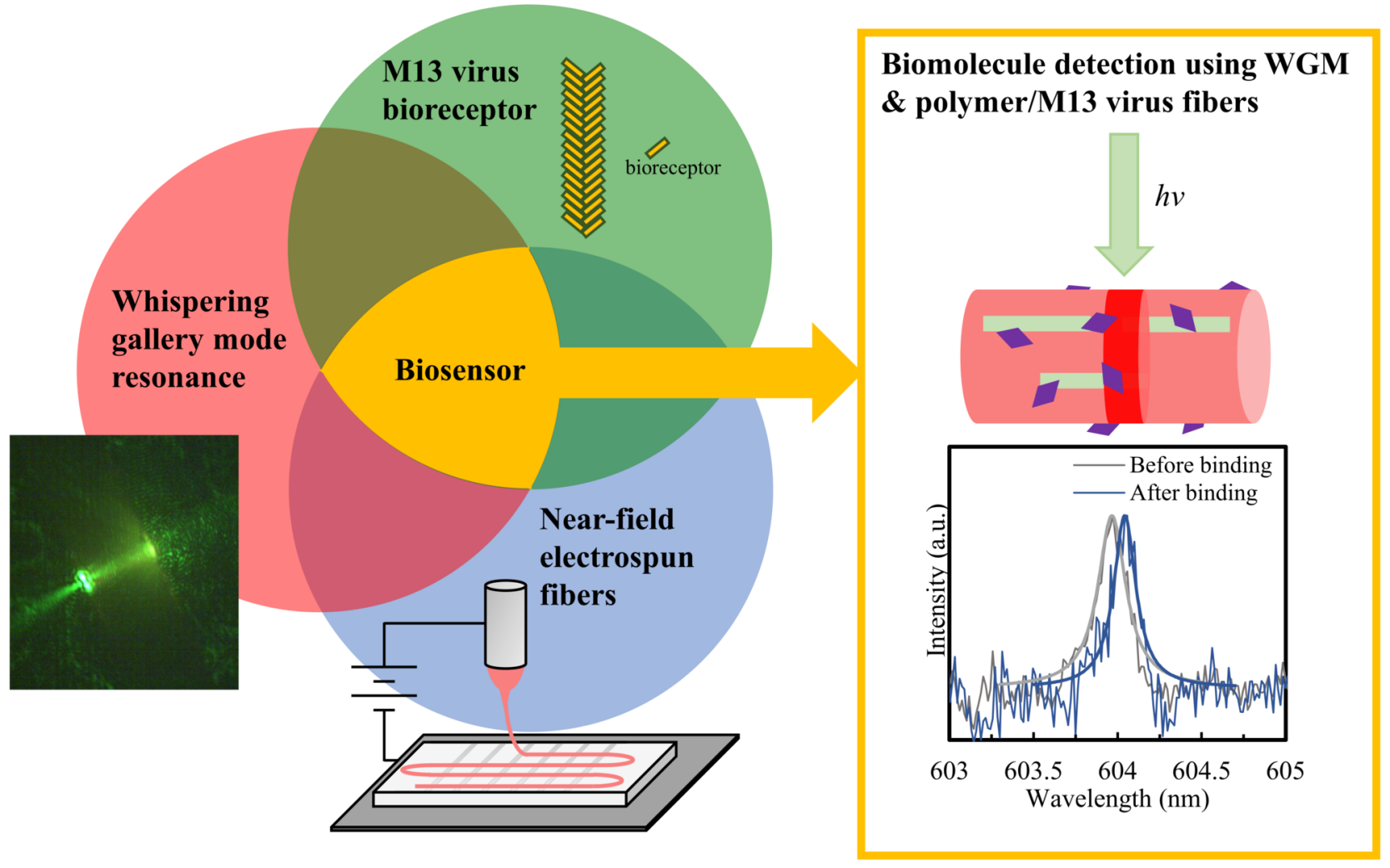
M13 virus bioreceptor
bioreceptor
Whispering gallery mode resonance
Biosensor
Near-field electrospun fibers
Biomolecule detection using WGM & polymer/M13 virus fibers
hv
Before binding
After binding
Intensity (a.u.)
603
603.5
604
604.5
605
Wavelength (nm)